Assessment of Radioactivity in Building Materials: Implications for Health in Kurdistan Region of Iraq

Adeeb O. Jafir[1†], Mohammed I. Hussein[1], Idrees A. Nadir[2], Barzan N. Sabr[1] and Ali H. Ahmed[1]

[1]Department of Physics, College of Science, Salahaddin University - Erbil, Erbil, Kurdistan Region – F.R. Iraq

[2]Department of Earth Sciences and Petroleum, College of Science, Salahaddin University - Erbil, Erbil, Kurdistan Region – F.R. Iraq

Abstract—**This research investigates the radioactivity levels of various rock types used in construction within the Kurdistan region and assesses their potential impact on human health, the measurements were performed using an HPGe gamma-ray spectrometer. The measured activity concentrations of ^{226}Ra, ^{232}Th, and ^{40}K radionuclides varied from ND (Chromitite) to 78.68 ± 4.54 Bq/kg (Marly Limestone), ND (Chromitite) to 109.52 ± 10.23 Bq/kg (Mudstone), and ND (Chromitite) to 2973.6 ± 152.1 Bq/kg (Claystone), respectively. The obtained Ra_{eq} values for all rock samples are well below the UNSCEAR, 2008 recommended value of 370 Bq/kg. 71.43% of D_R, 66.66% of E_{out}, 71.43% of E_{in}, 100% of H_{in} and H_{out}, 71.43% of $ELCR_{out}$, 71.43% of $ELCR_{in,}$ and 100% of activity utilization index of the rock samples are well below the recommended values declared by UNSCEAR, 2008. The radioactivity level of rock types that are prepared as building materials should be assessed by the producers and considered by the users to reduce the overall cancer risk. The outcomes of the RESRAD-BUILD computer code indicate that the maximum external and inhalation doses were calculated to be 19.7 and 0.105 μSv for R7 and R1 samples, respectively, over a period of 70 years.**

Index Terms **– Annual dose, Building materials, HPGe detector, Primordial radionuclides, Radiation indices, RESRAD-BUILD code, Rocks.**

I. Introduction

Radiation is present in the environment, and people are exposed to it in their natural environments through frequent sources of ionizing radiation. Background radiation typically comes from terrestrial and cosmic rays (Guidebook, 1989). The most common radionuclides in nature that produce gamma radiation are thorium, uranium, and potassium. Potassium experiences a simple radioactive decay, but uranium and thorium go through a series of complex disintegrations (Hanfi, et al., 2021).

The fundamental source of radiological exposure that monitors interest is due to primordial radionuclides such as ^{238}U, ^{232}Th, and ^{40}K, which occur in minerals such as zircon and monazites (Gaafar, Cuney, Gawad, 2014).

Uranium and thorium produce oxygen-containing compounds. Typically, 2–4 ppm of uranium and 8–12 ppm of thorium can be found in the crust of the earth. The minerals with the highest thorium concentrations in rocks are monazite, orthite, zircon, sphere, epidote, and apatite (El Mezayen, et al., 2019).

Potassium is the major element and thorium is the minor element by weight content in the Earth's crust (2.83% and 9.6 ppm, respectively). The origin of radon in minerals in the crust of the earth is the decay of uranium and thorium; the concentration increases in fractures and veins (Gundersen, 2020).

The rocks are used for different building purposes, such as cement (limestone) and construction material (sandstone), which are both sedimentary sources; bath scrub (pumice) and kerb stone (granite), which are both of igneous sources; roofing material (slate), which is of metamorphic source; and statues, ornaments, and adornments (marble), which are all made from metamorphic rocks (Hossain, et al., 2020).

As the public's anxiety grows, numerous studies have been conducted recently to evaluate the natural primordial radionuclides present in different rock types used as building materials locally and internationally (Ahmed and Hussein, 2011; Legasu and Chaubey, 2022; Alshahrani, 2021; Salaheldin, et al., 2020; Abbas, Khattab and Abdel Azeem, 2018; Harb, et al., 2012a; Alnour, et al., 2012; Harb, et al., 2012b; Turhan, 2010; Rosianna, et al., 2020; Kuzmanović, et al., 2020; Oladunjoye, et al., 2022; Narloch, et al., 2019; Fallatah and Khattab, 2023).

In Iraq, especially within the Kurdistan area, there is no level of reference for radioactivity, and the majority of the population has constructed their dwellings from a variety of materials derived primarily from rocks.

ARO-The Scientific Journal of Koya University
Vol. XII, No 2 (2024), Article ID: ARO.11545. 10 pages
DOI: 10.14500/aro.11545
Received: 08 February 2024; Accepted: 25 June 2024
Regular research paper; Published: 25 July 2024
†Corresponding author's e-mail: adeeb.jafir@su.edu.krd

The samples in the study area are composed of igneous, metamorphic, and sedimentary rocks (Table I), deposited at different geological ages from the Mesozoic to the Cenozoic. Tectonically, the study area is within the unstable shelf, and this zone is divided into subdivisions: thrust zone, imbricated zone, and high folded zone (Jassim and Goff, 2006).

In this study, the natural radioactivity of various rock types in the Kurdistan region of Iraq is determined using an HPGe gamma-ray spectrometer. Based on guidelines issued by UNSCEAR 2008, radium equivalent activities, the absorbed dose rate, annual effective dose, external and internal hazard index, activity utilization index (AUI), and excess lifetime cancer have been determined. In addition, the residents' inhalation and external doses have been computed using the simulation RESRAD BUILD computer code. Aiming to inform safety standards and mitigate health risks associated with prolonged exposure to natural radionuclides.

II. Geological Setting of the Study Area

Tectonically, Iraq is divided into many NW-SE trending parallel zones, according to Jassim and Goff, 2006. Iraq is tectonically divided from the southwest to the northeast into two major units: The Arabian Platform and the Shalair (Sanandaj-Sirjan) Terrane. The Arabian Platform is divided into an inner and an outer platform. The inner platform corresponds to the southwestern part of the stable shelf, whereas the outer platform was divided into the Mesopotamia Foredeep and the Western Zagros Fold-Thrust Belt. The Western Zagros Fold-Thrust Belt is further divided into four zones: The Low-Folded Zone (equivalent to the Foothill Zone), the High-Folded Zone, the Imbricate Zone, and the Suture Zone (Jassim and Goff, 2006). The geological map of the study area is shown in Fig. 1.

III. Materials and Procedures

A. Collection and Processing of Samples

In this investigation, 21 different types of rocks (three samples from each position and taking the average reduce the statistical uncertainty and improve the stability) were gathered from different locations in Kurdistan, as depicted in Fig. 2. All of the samples were pulverized and ground to the proper grain size for a 100-mesh sieve, and then desiccated in a furnace at 110°C for approximately 24 h. To establish secular equilibrium among the parent and its progeny, the dried samples were set within a 1 L Marinelli beaker with a tightly taped and sealed neck to prevent radon gas from escaping and then stored for 4 weeks.

In addition to the longitude, latitude, and altitude obtained using the GPS model (GPS-72, GARMIN), the geological character and elevation above sea level at each location have been determined, as illustrated in Table I.

B. Estimation of Primordial Radionuclides in Rock Samples

The activity concentration of radionuclides was obtained from the spectra. In this configuration, Princeton Gamma Tech (PGT) Corporation, United States, manufactured the high-purity germanium detectors consisting of a vertically closed-end p-type coaxial with the following features: The diameter and length of the crystal are 70.6 and 70.7 mm, respectively (Azeez, Ahmad and Mansour, 2018).

Both resolution and relative efficiency for the detector were 1.97 keV for the second photopeak of ^{60}Co and 73.8%, respectively. The system's energy was calibrated using man-

TABLE I

Geological and Geographical Information about the Study Area

Sample code	Location	Rock type	Rock components	Longitude	Latitude	Elevation (m)
R1	Bastora	Mudstone	Clay minerals	36°19'58" N	44°10'07" E	620
R2	Banaman	Sandstone	Quartz, feldspar, and rock fragments	36°21'14" N	44°10'47" E	740
R 3	Banaman	Marly limestone	Claystone and calcite	36°21'14" N	44°10'55" E	750
R 4	Banaman	Chalky limestone	calcite	36°21'30" N	44°11'20" E	800
R 5	Banaman	Dolomitic limestone	Dolomite mineral and calcite	36°21'30" N	44°11'20" E	800
R 6	Kore	Gypsum	Gypsum minerals	36°23'59" N	44°15'12" E	820
R 7	Kore	Claystone	Clay minerals	36°23'59" N	44°15'12" E	820
R 8	Hujran	Siltstone	Quartz and feldspar	36°24'27" N	44°15'45" E	830
R 9	Hujran	Marlstone	Clay minerals and calcite	36°24'48" N	44°15'48" E	830
R 10	Hujran	Limestone	Calcite	36°25'12" N	44°15'54" E	860
R 11	Beklo	Gabbro	Pyroxene, Ca-plagioclase, and Olivine	36°07'13" N	45°16'20" E	1215
R 12	Qalandar	Chromitite	Chromite mineral and serpentine	36°48'33" N	44°27'00" E	1345
R 13	Beklo	Amphibolite	Homblend and plagioclase	36°08'20" N	45°17'25" E	1421
R 14	Jinasan	Pyroxenite	Pyroxene 100%	36°37'08" N	44°55'07" E	1468
R 15	Penjween	Hornblendite	Hornblende 100%	35°34'56" N	45°58'02" E	1469
R 16	Qaladiza	Marble	calcite	36°07'54" N	45°16'42" E	915
R 17	Shler valley	Plagiogranite	Quartz, Na-plagioclase, and orthoclase	35°45'59" N	46°12'09" E	1400
R 18	Shler valley	Granite	Quartz, orthoclase and Na-plagioclase	35°48'02" N	46°13'46" E	1920
R 19	Shler valley	Metamorphosed granite	Quartz, orthoclase, and Na-plagioclase	35°46'07" N	46°16'58" E	1630
R 20	Shler valley	Metamorphosed granite with increasing iron deposits	Quartz, orthoclase, and Na-plagioclase+Iron	35°46'04" N	46°17'36" E	1840
R 21	Choman	Phyllite	Clay minerals	36°34'49" N	44°59'29" E	3288

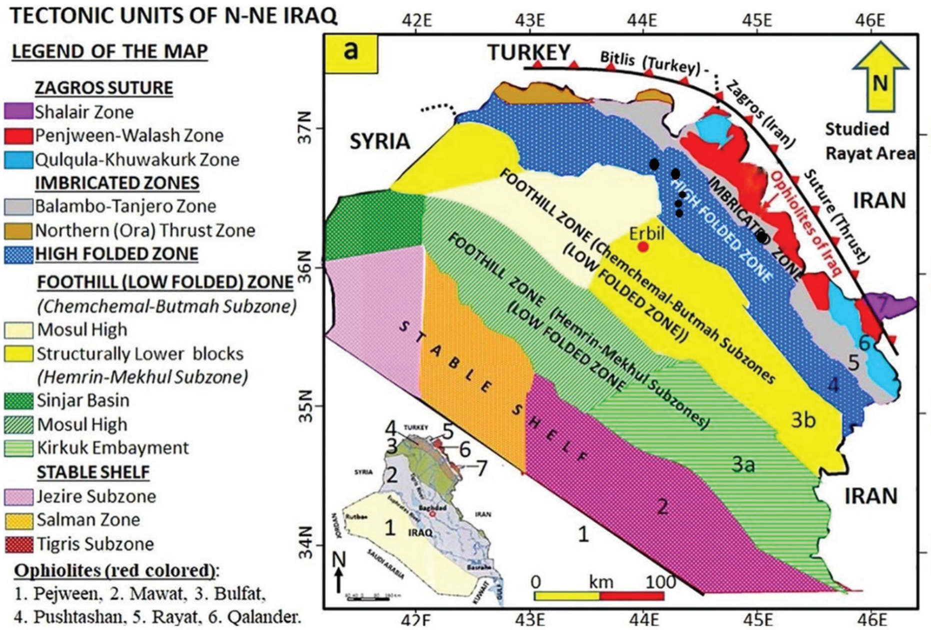

Fig. 1. Tectonic map of Iraq shows the study area (Ahmed, Kettanah and Ismail, 2020).

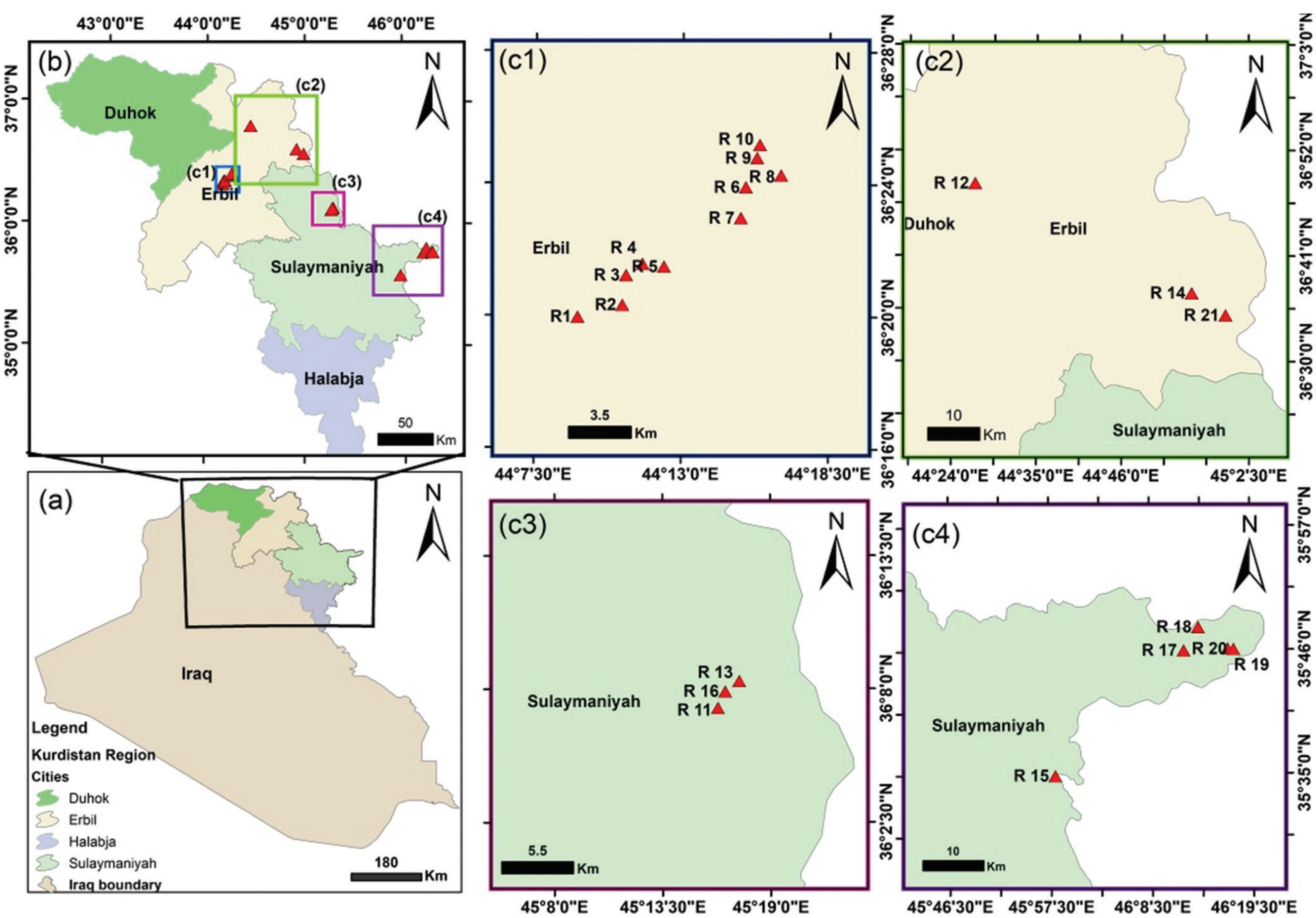

Fig. 2. Sampled position area in the Kurdistan Region.

made sources of ^{60}Co, ^{137}Cs, and ^{226}Ra. The standard sources used for the efficiency calibration must be under the same conditions as rock samples (Abdel-Rahman, et al., 2018; Bell, Judge and Regan, 2012).

The gamma spectroscopy technique of the HPGe detector at Koya University was used to obtain the spectra of rock samples. Both KCL and $UO_2(OCOCH_3)_2 2H_2O$ in powder and solution form were applied to the volumetric efficiency curves of Angle-3 with satisfaction (Azeez, Ahmad and Mansour, 2018).

To minimize the radiation that originates from the environmental background, the detector was enclosed in a lead that was 10 cm thick. The samples were left on the detector for 10 h. Using software developed for computers (Quantum-Gold for the PGT Corporation, 2001) and an 8000 multichannel analyzer, the spectra were obtained (Smail, Mansour and Ahmad, 2023). The activity concentration of ^{226}Ra was obtained from the weighted average of both ^{214}Pb and ^{214}Bi decay with energies of 351.9 keV and 609.3 keV, respectively, whereas ^{232}Th was obtained from ^{212}Pb, ^{208}Ti, and ^{228}Ac with energies of 583, 2614.5, and 911.2 keV, respectively. In addition, ^{40}K was determined from 1460.8 keV (10.7%). For the activity concentrations (A_C) of primordial radionuclides in rock samples, the following equation was used: (Jafir, 2023):

$$A_C\ (Bq\ kg^{-1}) = N\ (\varepsilon \times \gamma \times m \times t)^{-1} \pm SD\ (\varepsilon \times \gamma \times m \times t)^{-1} \quad (1)$$

Where N, ε, γ, m, t, and standard deviation are the net area under the photo peak after being subtracted from background, efficiency, branching ratio, mass, time, and standard deviation, respectively.

For primordial radionuclides, the minimum detectable activities (MDA) were obtained using the following formula (Dina, et al., 2022):

$$\mathrm{MDA} = 1.645\sqrt{b}\ (\varepsilon \times \gamma \times m \times t)^{-1} \quad (2)$$

Where b and 1.645 are background counts and statistical coverage factors at a specified level of confidence of 95%, respectively. The calculated MDA for ^{226}Ra, ^{232}Th, and ^{40}K were found to be 0.54, 0.55, and 0.83 Bq/kg, respectively.

IV. Radiological Indices

Measurement and evaluation of radiological indices are required to emphasize the radioactive dangers resulting from the presence of radionuclides in rocks.

A. Radium Equivalent (Ra_{eq})

Due to the asymmetrical distribution of primordial natural radionuclides in rock samples (Legasu and Chaubey, 2022). It was established that the activity concentrations of ^{226}Ra, ^{232}Th, and ^{40}K may be mathematically expressed as a single parameter of (Ra_{eq}).

$$Ra_{eq}\ (Bq\ kg^{-1}) = A_{Ra} + A_{Th} \times 1.41 + A_K \times 0.077 \quad (3)$$

Where A_{Ra}, A_K, and A_{Th} represent the radium, thorium, and potassium-specific activities, respectively.

B. Absorbed Gamma Dose Rate (D_R)

The absorbed dose rate produced by evenly dispersed naturally existing radionuclides ^{226}Ra, ^{232}Th, and ^{40}K at a height of 1 m over the ground's surface was computed in accordance with the guidance stated by the UNSCEAR, 2000. The following relationship is used to calculate the absorbed gamma dose rate (on the Effects of Atomic Radiation and others, 2008) (Dina, et al., 2022):

TABLE II
Activity Concentrations of Primordial Radionuclides in Different Rock Samples

Sample code	Activity concentration (Bq/kg)		
	^{226}Ra	^{232}Th	^{40}K
R1	28.84±3.54	109.52±10.23	1382.10±75.12
R2	25.06±2.66	50.64±4.77	1544.90±67.19
R3	78.68±4.54	7.71±2.53	494.20±32.03
R4	22.83±2.53	ND±ND	181.9±19.41
R5	ND±ND	1.19±0.69	ND±ND
R6	ND±ND	ND±ND	4.06±0.76
R7	31.50±3.94	15.21±2.52	2973.60±152.1
R8	3.41±0.32	ND±ND	62.22±2.94
R9	36.49±3.47	13.58±3.52	683.60±43.74
R10	41.75±3.87	23.07±4.38	2559.60±120.80
R11	ND±ND	ND±ND	43.96±3.50
R12	ND±ND	ND±ND	ND±ND
R13	1.98±0.31	9.5±0.51	9.65±1.27
R14	5.77±1.35	13±1.59	52.64±6.57
R15	8.08±1.48	10.57±1.96	261.7±17.89
R16	2.38±0.81	ND±ND	ND±ND
R17	ND±ND	1.07±0.34	32.62±4.39
R18	23.16±3.04	58.43±5.94	1319.5±72.04
R19	32.74±3.36	65.82±5.89	2013.20±95.44
R20	11.71±1.77	12.18±2.08	423.80±24.9
R21	4.82±0.72	3.02±0.66	107.90±6.18

$$D_R\ (nGy\ h^{-1}) = A_{Ra} \times 0.462 + A_{Th} \times 0.604 + A_K \times 0.0417 \quad (4)$$

C. Annual Effective Dose Rate (E_{in} and E_{out})

The dose conversion factor (0.7) and the indoor occupancy factor (0.8), assuming 80% of the time is spent inside, are utilized for calculating the indoor annual effective dose rates (Qureshi, et al., 2014). This information comes from UNSCEAR. The annual effective dose (mSv/y) that a building resident would receive as a result of the activity within the rock materials was calculated using the following formula (Legasu and Chaubey, 2022):

$$E_{in}\ (mSv/y) = D_R \times 8760 \times 0.8 \times 0.7 \times 10^{-6} \quad (5)$$

In a similar way, the outdoor annual effective dose (E_{out}) is derived from the total gamma radiation dose rate (D_R) absorbed in rock samples by factoring in the outside occupancy factor of 0.2 and converting the factor from the rate of dose absorbed within air to the effective dose for individuals, which is 0.7 $Sv.Gy^{-1}$. UNSCEAR (2000) provided the following equation for calculating E_{out}:

$$E_{out}\ (mSv\ y^{-1}) = D_R \times 8760 \times 0.2 \times 0.7 \times 10^{-6} \quad (6)$$

D. AUI

The AUI is an index that may be used to determine whether a material is suitable for building construction or not, given that the material has dual impacts and may be utilized as both a radiation shield and a source of radiation. It is an indicator of the mass percentage of construction materials in a building that is proportional to the fractional usage of those materials. (AUI) is computed using the formula below (Qureshi, et al., 2014; Jafir, Ahmed and Saridan, 2018):

$$AUI = \left(A_{Ra} / 50\,Bq\,Kg^{-1}\right) f_{Ra} + \left(A_{Th} / 50\,Bq\,Kg^{-1}\right) f_{Th} + \left(A_K / 500\,Bq\,Kg^{-1}\right) f_K \tag{7}$$

Where f_{Ra} (0.462), f_{Th} (0.604), and f_K (0.0417) represent the relative contributions of the three radionuclide activities to the gamma dose amount within air.

V. Results and Discussion

Table II displays the results of the gamma-ray activity concentrations of ^{226}Ra and ^{232}Th, as well as the single decay scheme of ^{40}K. Concentrations of gamma-ray radionuclide activity are depicted in Fig. 3. Chromitite had the lowest concentrations of ^{226}Ra, ^{232}Th, and ^{40}K, all of which were below detection (ND). Maximum activity concentrations of ^{226}Ra, ^{232}Th, and ^{40}K were found in marly limestone (78.68 ± 4.54 Bq/kg), mudstone (109.52 ± 10.23 Bq/kg), and clay stone (2973.6 ± 152.1 Bq/kg), respectively. The absence of primordial radionuclides in chromitite rock types is related to the mineral composition, formation process, geological settings, and chemical differentiation.

When these results are compared to the global average value, the activity concentration of ^{226}Ra for all studied samples is within the same range as the global average (32 Bq/kg) stated by the (on the Effects of Atomic Radiation and others, 2008), with the exception of 14.28%, which is found in marly limestone (R3), marlstone (R9), and limestone (R10). For ^{232}Th activity concentration, 19% of the rock samples exceed the value of 45 Bq/kg, as in mudstone (R1), sandstone (R2), granite (R18), and metamorphosed granite (R19). Compared to UNSCEAR, 2008 (400 Bq/kg), it was found that 42.8% of the rock samples had higher ^{40}K activity concentrations. Long-term inhalation exposure to uranium and thorium can cause several health problems, including anemia, acute leucopenia, chronic lung illnesses, and oral

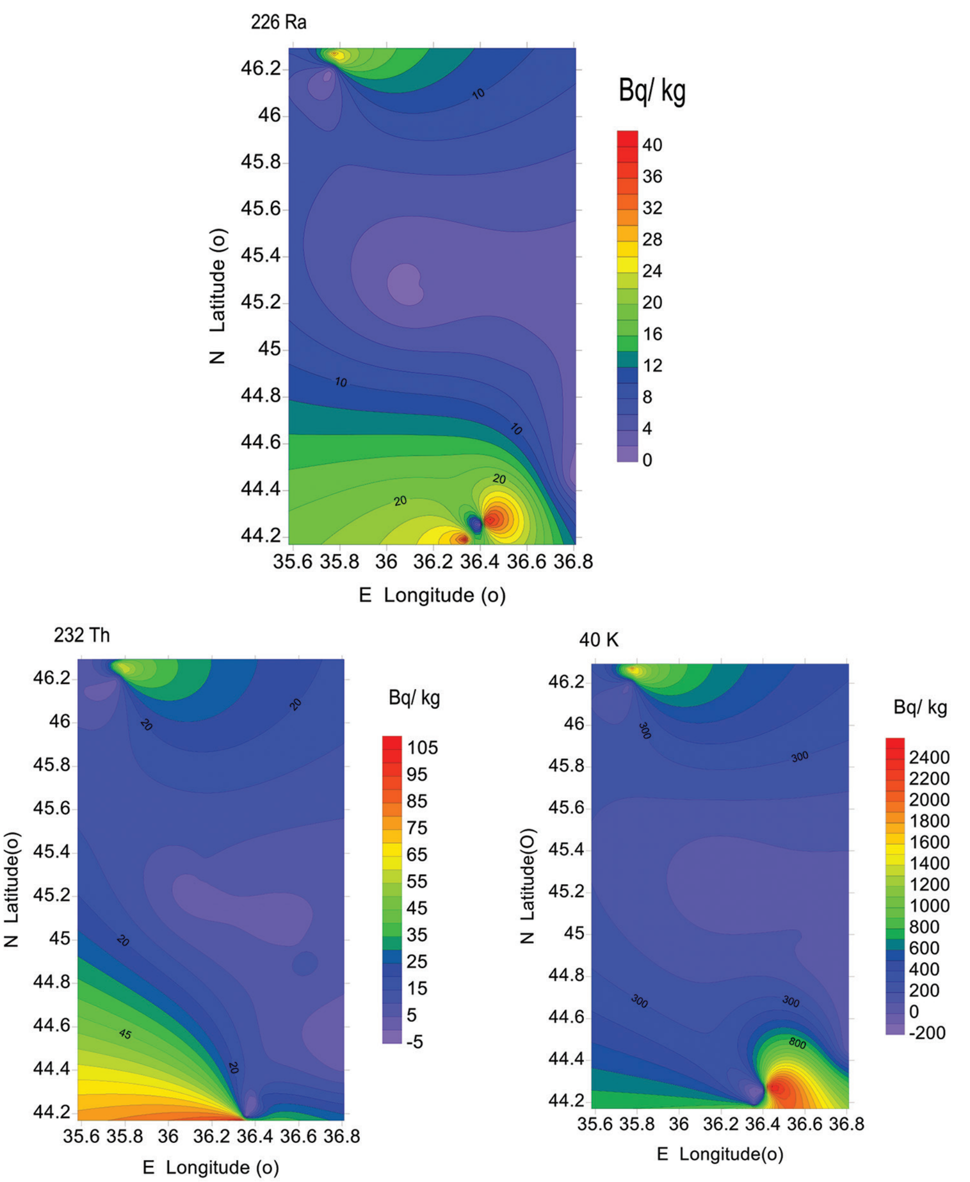

Fig. 3. Contour maps for activity concentrations of primordial radionuclides in rock samples.

 http://dx.doi.org/10.14500/aro.11545

necrosis. Cancers of the lungs, pancreas, liver, and kidneys can result from exposure to thorium (Taskin, et al., 2009).

Table III compares the obtained activity concentration values for ^{226}Ra, ^{232}Th, and ^{40}K with those observed in different countries. The radioactivity of sandstone samples is comparable to the same results reported in Bangladesh (Jaintapur region) (Dina, et al., 2022), but different from the same rock types in Egypt (Harb, et al., 2012a), the discrepancy in data between the two countries is due to the use of different detectors. For example, HPGe and NaI detectors are used. For the gypsum sample, our results are comparable to those reported in Turkey (Turhan, 2010) and Brazil (Narloch, et al., 2019) and lower than those in Iran (Imani, et al., 2021) and the use of gypsum in construction is safe and below the standard values in all of the countries mentioned. In the case of the siltstone samples, the results are completely different and considerably lower than those reported in Egypt (Harb, et al., 2012a). The results for limestone samples are completely inconsistent with those from Turkey (Turhan, 2010), particularly for the ^{40}K concentrations. Inconsistent with prior measurements from the Western Alps in France (Malczewski and Żaba, 2012), the outcomes obtained in this study for marble samples fall within the limits stated in the UNSCEAR 2008, report. The activity concentrations in granite samples are less than those reported in Egypt (Harb, et al., 2012a) and Malaysia (Alnour, et al., 2012) for ^{226}Ra, comparable for ^{232}Th, and greater than that for ^{40}K, but less than those reported in Nigeria (Oladunjoye, et al., 2022) and Saudi Arabia (Fallatah and Khattab, 2023) for ^{226}Ra and ^{232}Th and greater than that for ^{40}K. The activity concentrations for ^{226}Ra, ^{232}Th, and ^{40}K in chromitite are below the detection limit (ND), which is completely different from the results reported for the same rocks in India (Srinivasa, Rangaswamy and Sannappa, 2019). Chromite deposits (ultrabasic rocks) are found in the ultrabasic rocks of many ophiolites (Büchl, Brügmann and Batanova, 2004). Potassium, uranium, and thorium content increase in igneous rocks with magmatic fractionation. This decreases in basic and ultrabasic rocks since these elements fall within the incompatible group, that is, they are related to components with large radii and high charges, which felsic rocks lack (Aydin, et al., 2006; Lasheen, et al., 2021). Considering the geological mineral composition of rock samples and the geographical conditions derived from different regions of the earth's crust, there is a wide variation in activity concentration in the same rock types around the earth.

A. Radiological Hazard Indices

The estimated radiological effects (radium equivalent, absorbed gamma dose rate, annual effective dose rate, and AUI are tabulated in Table IV and depicted in Fig. 4.

TABLE III
COMPARES CURRENT STUDY ACTIVITY CONCENTRATIONS TO THOSE IN DIFFERENT COUNTRIES

Country	Rock type	Activity concentration (Bq/kg)			References
		$^{22}6$Ra	^{232}Th	^{40}K	
Saudi Arabia	Pumice	79.03	73.13	521.91	(Alshahrani, 2021)
Saudi Arabia	Granite	102.5	486.8	726	(Fallatah and Khattab, 2023)
Iraq (Kurdistan)	Basalt	5.65±0.22	21.4±1.78	203.34±8.12	(Ahmed and Hussein, 2011)
Egypt	Granite	45.75±2.28	50.91±2.56	826.13±39.33	(Salaheldin, et al., 2020)
Egypt	Sand-siltstone	88.8	458.8	627.5	(Abbas, Khattab and Abdel Azeem, 2018)
Egypt	Gneiss	28.4±3	37.7±4	1167.6±42	(Harb, et al., 2012a)
	Granite	118±7	90.5±7	2208±91	
	Basalt	59.5±4	67.7±6	718.5±42	
	Sandstone	7.5±1.5	12.5±3	263.9±11	
	Siltstone	113±7	148.5±12	1672±55	
Brazil	Natural gypsum	1.91±0.10	1.14±0.06	ND	(Narloch, et al., 2019)
Malaysia	Granite	39±0.7	52±1	611±15	(Alnour, et al., 2012)
Iran	Gypsum	12	14	116	(Imani, et al., 2021)
	Granite	38	47	917	
	Marble	7	7	34	
Yemen	Basalt	21.79±3.1	19.5±2.6	399.3±16	(Harb, et al., 2012b)
Turkey	Gypsum	7.2	3.4	40.7	(Turhan, 2010)
	Limestone	19	4.3	55	
Indonesia	Volcanic	22882±16	33549±23	1909±134	(Rosianna, et al., 2020)
China	Granite	356	318	1636	(Tuo, et al., 2020)
Serbia	Granite	200±89	77±6	1280±78	(Kuzmanović, et al., 2020)
Nigeria	Granite	130±20	352±41	412±119	(Oladunjoye, et al., 2022)
Western Alps, France	Calcschist	14.4	14.4	392	(Malczewski and Żaba, 2012)
	Carbonaceousbreccia	22.5	4.26	111	
	Limestone dolomite	26.2	0.52	18	
	Dolomite	29.0	3.0	129	
	Marble	25.7	1.63	78	
	Quartzite	9.1	8.3	572	
India (Karnataka)	Chromite	51.9±1.3	79.4±1.6	423.9±9.6	(Srinivasa, Rangaswamy and Sannappa, 2019)
Bangladesh (Jaintiapur area)	Sandstone	25±2	37±4	884±41	(Dina, et al., 2022)
World average	Background	32	45	400	(On the Effects of Atomic Radiation and others, 2008)

TABLE IV
The Estimated Radiation Hazard Indices for the Rock Samples

Rock types	Ra_{eq}. Bq/kg	D_R (nGy/h)	E_{out} (mSv/y)	E_{in} (mSv/y)	AUI
R1	291.87	137.11	0.17	0.67	1.70
R2	216.43	106.58	0.13	0.52	0.97
R3	127.75	61.61	0.08	0.30	0.86
R4	36.83	18.13	0.02	0.09	0.23
R5	1.70	0.72	0.00	0.00	0.01
R6	0.31	0.17	0.00	0.00	0.00
R7	282.21	147.74	0.18	0.72	0.72
R8	8.20	4.17	0.01	0.02	0.04
R9	108.54	53.56	0.07	0.26	0.56
R10	271.83	139.96	0.17	0.69	0.87
R11	3.38	1.83	0.00	0.01	0.00
R12	ND	ND	ND	ND	ND
R13	16.31	7.05	0.01	0.03	0.13
R14	28.42	12.72	0.02	0.06	0.21
R15	43.35	21.03	0.03	0.10	0.22
R16	2.38	1.10	0.00	0.01	0.02
R17	4.04	2.01	0.00	0.01	0.02
R18	208.32	101.02	0.12	0.50	1.03
R19	281.87	138.83	0.17	0.68	1.26
R20	61.76	30.44	0.04	0.15	0.29
R21	17.44	8.55	0.01	0.04	0.09
World average	370	59	0.07	0.41	2

In the current study, the Ra_{eq} varied from ND (R12) to 291.87 Bq/kg (R1), as depicted in Fig. 4. The obtained values are lower than the suggested maximum of 370 Bq/kg (Annex, 2000).

The estimated absorbed dose rate ranges from ND (R12) to 147.74 nGy/h (R7); the maximum values are nearly twice the worldwide mean value of 59 nGy/h (Annex, 2000; Jafir, 2023), indicating that 28.57% of the calculated absorbed dose rate resulting from natural radioactive nuclides within the air for the studied area is above the allowed internationally recommended value. The outdoor annual effective doses of the public in the Kurdistan region due to exposure range from ND (R12) to 0.18 mSv/y (R7), whereas the indoor annual effective doses varied from ND (R12) to 0.72 mSv/y (R7), which indicates that 33.34% and 28.57% of the rock samples are outside the range of 0.07 mSv/y and 0.41 mSv/y for both types, respectively, as declared by (on the Effects of Atomic Radiation and others, 2008).

The obtained AUI values range from ND (R12) to 1.70 (R1). All are <2, implying an effective annual dose of a value below 0.3 mSv/y (Jafir, Ahmed and Saridan, 2018). The result demonstrates that these rocks are suitable for use in construction. Similar results were obtained by (Raghu, et al., 2017) regarding construction materials.

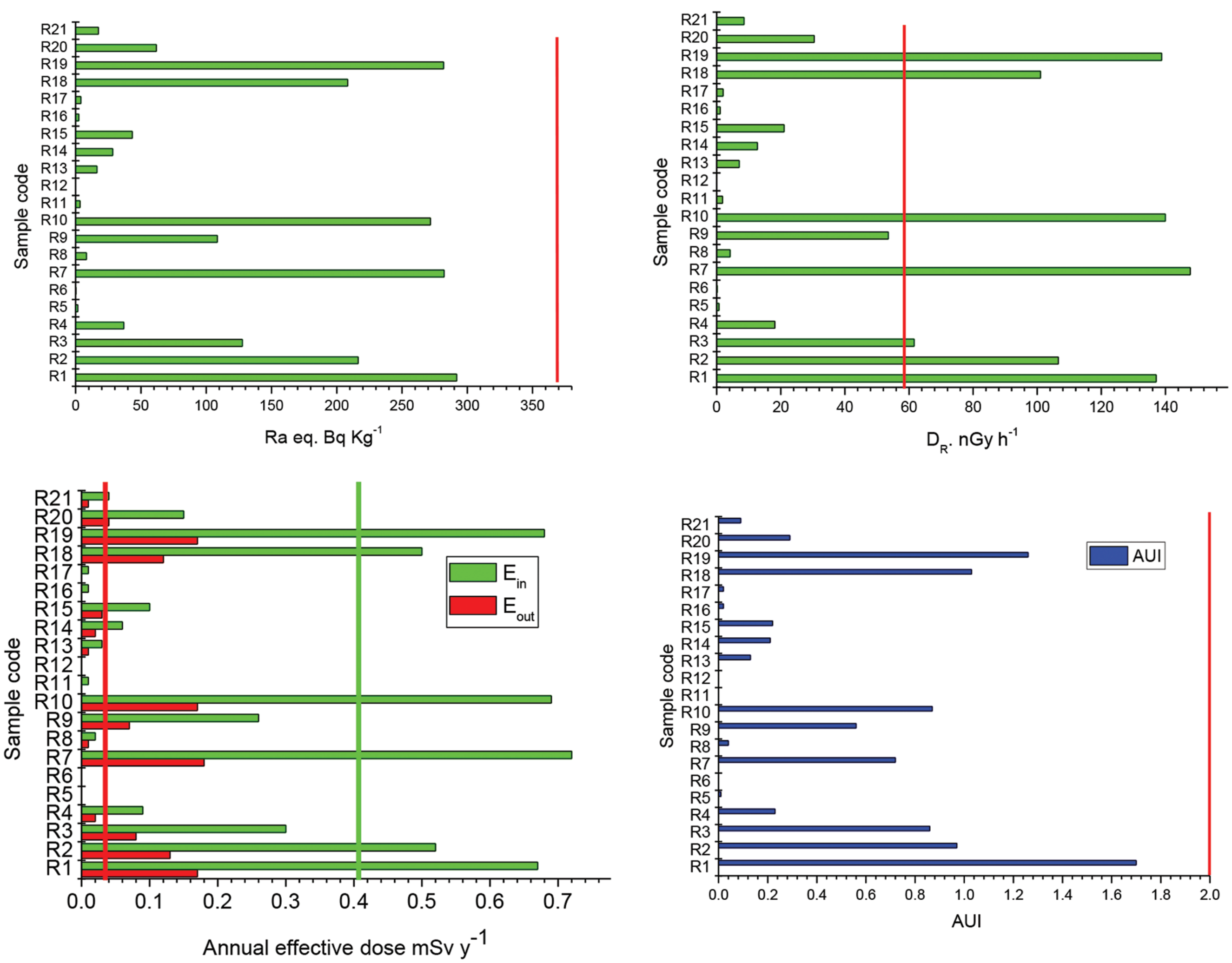

Fig. 4. The estimated radiation hazard indices for the rock samples.

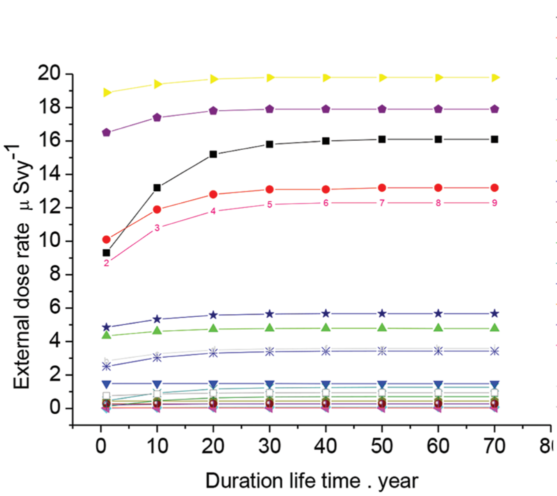

Fig. 5. Long-term variation in the external dose rate that individuals in a standard room are exposed to for all rock samples.

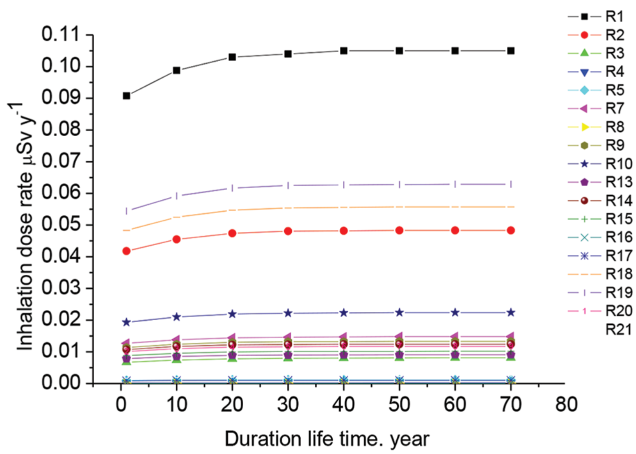

Fig. 6. Long-term variation in the inhalation dose rate that individuals in a standard room are exposed to for all rock samples.

B. RESRAD BUILD Simulation

About 80% of the inhabitants' time is spent indoors, so they might be significantly impacted by the natural radioactivity that emanates from the components of building materials. It is possible to calculate the radiological indoor dose of a resident of a radioactively contaminated building using the RESRAD-BUILD code (Yu, et al., 1994).

Room dimensions scenario

To investigate the impacts of the rocks used to construct the building's walls, the thickness of the walls was fixed at 20 cm, and the room dimensions were fixed at (3 × 6 × 3) m. The annual external and inhalation dose rates were computed over 70 years. The rocks' density was 1.51 g/cm^{-3}. For this scenario, the default values for the inhalation rate of 18 m^3/day, deposition velocity of 0.01/ms, ingestion rate of 0.0001 m^2/h, and resuspension rate of 0.0000005/s were applied. The input activity concentrations of ^{226}Ra, ^{232}Th, and ^{40}K for RESRAD-BUILD simulations are listed in Table II.

External dose rate

Fig. 5 depicts the calculated external exposures for all samples over an average period of 70 years. During the first 30 years, the external indoor doses increased significantly before becoming reasonably saturated. Maximum external doses over 70 years were observed to be 19.7 μSv in the R7 sample; compared to the R10 sample, the activity concentrations of ^{226}Ra and ^{232}Th are lower in R10, whereas the activity concentration of ^{40}K is higher, reflecting the fact that the cases were controlled by the high activity concentrations of ^{40}K. All measured values are well below the UNSCEAR 2000 critical value of 2.6 mSv/y. This is consistent with the results of previous investigations (Adelikhah, et al., 2022).

Inhalation indoor dose rate

The calculated indoor inhalation doses for all samples and the average period of 70 years are presented in Fig. 6. During the first 30 years, indoor inhalation doses increased significantly before becoming relatively constant. The R1 exhibited the highest indoor inhalation doses due to the high activity concentrations of ^{226}Ra and ^{232}Th, respectively. Compared to the activity concentration in R10 samples, radon originates from ^{226}Ra (^{222}Rn) and ^{232}Th (^{220}Rn), whereas ^{40}K does not contribute to dose inhalation (Adelikhah, et al., 2022; Ndjana Nkoulou 2nd, et al., 2022). This inhalation dose range is lower than the global average of 5.799 μSv/y (Annex, 2000). The low level of radon concentration in building materials over 70 years is due to continuous changes in the air exchange rate. Mudstone (R1) has the greatest inhalation dose among the 21 studied rocks, while R12 has the lowest (zero) inhalation dose delivered to the inhabitants.

VI. Conclusion

The calculated activity concentrations of primordial radionuclides ^{226}Ra, ^{232}Th, and ^{40}K fall within the range declared by UNSCEAR (2008), with the respective exception ratios of 14.28%, 19%, and 42.8% for the studied rock samples. The determined activity concentrations and radiological hazards in the rock types can be used as baseline data to determine any future radiological changes resulting from environmental and human activities. The lowest amount of Ra_{eq} was found in chromitite, whereas the greatest amount was identified in mudstone. A wide variation of activity concentration was observed in different rock types, the result of the present study indicates that individuals should be aware of the potential radiological risks of utilizing rocks as building materials before using them and that long-term exposure to low doses of radiation in rock samples can increase the overall risk of cancer. According to the results obtained from RESRAD simulations, the indoor dose was controlled by ^{232}Th compared to ^{226}Ra due to the homogenous condition for both ^{222}Rn and ^{220}Rn in the standard model of the room; the short lifetime of ^{220}Rn (56 s) reflects the uncertainty in the homogeneity. Finally, because the RESRAD-BUILD takes into account both radionuclide decay and the ingrowth of the decay product, the ingrowth of the ^{232}Th decay product may cause the dosage to look higher, but ^{226}Ra is not an issue because it reaches equilibrium much faster. The results also show that ^{40}K controlled the external dose rate, but it did not contribute to the indoor dose due to its long half-lives. Furthermore, the rocks used in the building construction would not contain pure ^{226}Ra or ^{232}Th, although they can have a distributed decay chain.

References

Abbas, A.E.H.A., Khattab, M.R., and Abdel Azeem, M.M., 2018. Natural radionuclides distribution and environmental impacts of ferruginous sand-siltstone (raw material) and their manufactured Ahmer oxide used as wall paints. *Environmental Forensics*, 19, pp.217-224.

Abdel-Rahman, M.A.E., El-Mongy, S.A., Farghal, A., and Sayed, M.S., 2018. Study of Some Parameters Affecting Efficiency of HpGe Detectors for Accurate Radionuclides Analysis. In: *The International Conference on Chemical and Environmental Engineering*. Military Technical College, Egypt, pp.371-388.

Adelikhah, M., Imani, M., Hegedhus, M., and Kovács, T., 2022. Modelling of indoor external and internal exposure due to different building materials containing NORMs in the vicinity of a HNBRA in Mahallat, Iran. *Heliyon*, 8, p.e08909.

Ahmed, A.A., and Hussein, M.I., 2011. Natural radioactivity measurements of basalt rocks in Sidakan district northeastern of Kurdistan region-Iraq. *International Journal of Geo-Engineering*, 5, pp.66-73.

Ahmed, I.N., Kettanah, Y.A., and Ismail, S.A., 2020. Genesis and tectonic setting of high-Cr podiform chromitites of the Rayat ophiolite in the Zagros Suture Zone, Northeastern Iraq. *Ore Geology Reviews*, 123, p.103583.

Alnour, I.A., Wagiran, H., Ibrahim, N., Laili, Z., Omar, M., Hamzah, S., and Idi, B.Y., 2012. Natural radioactivity measurements in the granite rock of quarry sites, Johor, Malaysia. *Radiation Physics and Chemistry*, 81, pp.1842-1847.

Alshahrani, B.E., 2021. Natural radioactivity level in pumice rock, in Saudi Arabia and effect on human health. *International Journal of Environmental Analytical Chemistry*, 103(14), pp.3410-3421.

Annex, A., 2000. *Dose Assessment Methodologies. Sources of Effects Ionizing Radiation*. UNSCEAR, Austria.

Aydin, I., Aydoğan, M.S., Oksum, E., and Koçak, A., 2006. An attempt to use aerial gamma-ray spectrometry results in petrochemical assessments of the volcanic and plutonic associations of Central Anatolia (Turkey). *Geophysical Journal International*, 167, pp.1044-1052.

Azeez, H.H., Ahmad, S.T., and Mansour, H.H., 2018. Assessment of radioactivity levels and radiological-hazard indices in plant fertilizers used in Iraqi Kurdistan Region. *Journal of Radioanalytical and Nuclear Chemistry*, 317, pp.1273-1283.

Bell, S.J., Judge, S.M., and Regan, P.H., 2012. An investigation of HPGe gamma efficiency calibration software (ANGLE V. 3) for applications in nuclear decommissioning. *Applied Radiation and Isotopes*, 70, pp.2737-2741.

Büchl, A., Brügmann, G., and Batanova, V.G., 2004. Formation of podiform chromitite deposits: implications from PGE abundances and Os isotopic compositions of chromites from the Troodos complex, Cyprus. *Chemical Geology*, 208, pp.217-232.

Dina, N.T., Das, S.C., Kabir, M.Z., Rasul, M.G., Deeba, F., Rajib, M., Islam, M.S., Hayder, M.A., and Ali, M.I., 2022. Natural radioactivity and its radiological implications from soils and rocks in Jaintiapur area, North-east Bangladesh. *Journal of Radioanalytical and Nuclear Chemistry*, 331, pp.4457-4468.

El Mezayen, A.M., Heikal, M.A., El-Feky, M.G., Shahin, H.A., Abu Zeid, I.K., and Lasheen, S.R., 2019. Petrology, geochemistry, radioactivity, and M--W type rare earth element tetrads of El Sela altered granites, south eastern desert, Egypt. *Acta Geochimica*, 38, pp.95-119.

Fallatah, O., and Khattab, M.R., 2023. Evaluation of environmental radioactivity and hazard impacts saudi arabia granitic rocks used as building materials. *Minerals*, 13, p.165.

Gaafar, I., Cuney, M., and Gawad, A.A., 2014. Mineral chemistry of two-mica granite rare metals: Impact of geophysics on the distribution of uranium mineralization at El Sela Shear Zone, Egypt. *Open Journal of Geology*, 4, p.137.

Guidebook, A., 1989. *Measurement of Radionuclides in Food and the Environment*. International Atomic Energy Agency, Vienna.

Gundersen, L.C.S., 2020. Radon in sheared metamorphic and igneous rocks. In: *Field Studies of Radon in Rocks, Soils, and Water*. Vol. 39. CRC Press, United States, pp.39-50.

Hanfi, M.Y.M., Masoud, M.S., Sayyed, M.I., Khandaker, M.U., Faruque, M.R.I., Bradley, D.A., and Mostafa, M.Y.A., 2021. The presence of radioactive heavy minerals in prospecting trenches and concomitant occupational exposure. *PLoS One*, 16, p.e0249329.

Harb, S., Abbady, A.E.B., El-Kamel, A.E.H., Saleh, I.I., and Abd El-Mageed, A.I., 2012a. Natural radioactivity and their radiological effects for different types of rocks from Egypt. *Radiation Physics and Chemistry*, 81, pp.221-225.

Harb, S., El-Kamel, A.E.H., Abbady, A.E.B., Saleh, I.I., and Abd El-Mageed, A.I., 2012b. Specific activities of natural rocks and soils at quaternary intraplate volcanism north of Sana'a, Yemen. *Journal of Medical Physics*, 37, p.54.

Hossain, M.F.A., Tasneem, N., Alam, A.B.M.R., and Hossain, A.S.M.F., 2020. Study on the properties and uses of rocks found in Bangladesh. *Soil Dynamics and Earthquake Engineering*, 3, pp.1-7.

Imani, M., Adelikhah, M., Shahrokhi, A., Azimpour, G., Yadollahi, A., Kocsis, E., Toth-Bodrogi, E., and Kovács, T., 2021. Natural radioactivity and radiological risks of common building materials used in Semnan province dwellings, Iran. *Environmental Science and Pollution Research*, 28, pp.41492-41503.

Jafir, A.O., 2023. Investigation of radioactivity level in drinking water resources and soil samples collected from the Hawraman villages, Iraq. *Applied Radiation and Isotopes*, 194, p.110665.

Jafir, A.O., Ahmed, A.H., and Saridan, W.M., 2018. Estimation of radiological parameters from seasonal observations of primordial natural radionuclides in sediments of Darbandikhan Lake water resources at Kurdistan region, Northeastern Iraq. *Environmental Earth Sciences*, 77, p.334.

Jassim, S.Z., and Goff, J.C., 2006. *Geology of Iraq*. DOLIN, s.r.o., distributed by Geological Society of London, p.5.

Kuzmanović, P., Todorović, N., Filipović Petrović, L., Mrda, D., Forkapić, S., Nikolov, J., and Knežević, J., 2020. Radioactivity of building materials in Serbia and assessment of radiological hazard of gamma radiation and radon exhalation. *Journal of Radioanalytical and Nuclear Chemistry*, 324, pp.1077-1087.

Lasheen, E.S.R., Rashwan, M.A., Osman, H., Alamri, S., Khandaker, M.U., and Hanfi, M.Y., 2021. Radiological hazard evaluation of some egyptian magmatic rocks used as ornamental stone: Petrography and natural radioactivity. *Materials* (*Basel*), 14, p.7290.

Legasu, M.L., and Chaubey, A.K., 2022. Determination of dose derived from building materials and radiological health related effects from the indoor environment of Dessie city, Wollo, Ethiopia. *Heliyon*, 8, p.e09066.

Malczewski, D., and Żaba, J., 2012. Natural radioactivity in rocks of the Modane--Aussois region (SE France). *Journal of Radioanalytical and Nuclear Chemistry*, 292, pp.123-130.

Narloch, D.C., Paschuk, S.A., Corrêa, J.N., Rocha, Z., Mazer, W., Torres, C.A.M.P., Del Claro, F., Denyak, V., and Schelin, H.R., 2019. Characterization of radionuclides present in portland cement, gypsum and phosphogypsum mortars. *Radiation Physics and Chemistry*, 155, pp.315-318.

Ndjana Nkoulou, J.E. 2nd, Manga, A., German, O., Sainz-Fernandez, C., and Kwato Njock, M.G., 2022. Natural radioactivity in building materials, indoor radon measurements, and assessment of the associated risk indicators in some localities of the Centre Region, Cameroon. *Environmental Science and Pollution Research*, 29, pp.54842-54854.

Oladunjoye, O.I., Yinusa, T.S., Ajekiigbe, K.M., and Oketayo, O.O., 2022.

http://dx.doi.org/10.14500/aro.11545

Assessment of radiation hazard indices caused by naturally occurring radionuclides in granite samples from selected quarry Site in Kano State, Northwest Nigeria. *Radiochemistry*, 64, pp.656-664.

Qureshi, A.A., Tariq, S., Din, K.U., Manzoor, S., Calligaris, C., and Waheed, A., 2014. Evaluation of excessive lifetime cancer risk due to natural radioactivity in the rivers sediments of Northern Pakistan. *Journal of Radiation Research and Applied Sciences*, 7, pp.438-447.

Raghu, Y., Ravisankar, R., Chandrasekaran, A., Vijayagopal, P., and Venkatraman, B., 2017. Assessment of natural radioactivity and radiological hazards in building materials used in the Tiruvannamalai District, Tamilnadu, India, using a statistical approach. *Journal of Taibah University for Science*, 11, pp.523-533.

Rosianna, I., Nugraha, E.D., Syaeful, H., Putra, S., Hosoda, M., Akata, N., and Tokonami, S., 2020. Natural radioactivity of laterite and volcanic rock sample for radioactive mineral exploration in Mamuju, Indonesia. *Geosciences*, 10, p376.

Salaheldin, G., El-Gamal, H., Zahran, E.B., and Abdel, M., 2020. Assessment of radiation hazards of radionuclides for granite rocks from Gabal Ghareb, Eastern Desert of Egypt. *Assiut University Journal of Multidisciplinary Scientific Research*, 49, pp.1-16.

Smail, J.M., Mansour, H.H., and Ahmad, S.T., 2023. Evaluation of radiological hazards in lower Zab river sediments. *Radiation Effects and Defects in Solids*, 178, pp.1252-1268.

Srinivasa, E., Rangaswamy, D.R., and Sannappa, J., 2019. Assessment of radiological hazards and effective dose from natural radioactivity in rock samples of Hassan district, Karnataka, India. *Environmental Earth Sciences*, 78, p.431.

Taskin, H., Karavus, M., Ay, P., Topuzoglu, A., Hidiroglu, S., and Karahan, G., 2009. Radionuclide concentrations in soil and lifetime cancer risk due to gamma radioactivity in Kirklareli, Turkey. *Journal of Environmental Radioactivity*, 100, pp.49-53.

The United Nations Scientific Committee on the Effects of Atomic Radiation (UNSCEAR), 2008. *Effects of Ionizing Radiation, United Nations Scientific Committee on the Effects of Atomic Radiation (UNSCEAR) 2006 Report*, *Volume I*: *Report to the General Assembly, Scientific Annexes A and B. United Nations*.

Tuo, F., Peng, X., Zhou, Q., and Zhang, J., 2020. Assessment of natural radioactivity levels and radiological hazards in building materials. *Radiation Protection Dosimetry*, 188, pp.316-321.

Turhan, S., 2010. Radioactivity levels of limestone and gypsum used as building raw materials in Turkey and estimation of exposure doses. *Radiation Protection Dosimetry*, 140, pp.402-407.

Yu, C., LePoire, D.J., and Jones, L.G., 1994. *RESRAD-BUILD: A Computer Model for Analyzing the Radiological doses Resulting from the Remediation and Occupancy of Buildings Contaminated with Radioactive Material*. The University of Chicago, Chicago.